Please cite the Published Version

Khan, Muhzamil A , Crapnell, Robert D , Bernalte, Elena , Riehl, Bill Logan, Rowley-Neale, Samuel J , and Banks, Craig E (2025) Exploring the Use of Different Carbon Materials Within Additive Manufactured Electrodes: The Sensing of Carbendazim. Electroanalysis, 37 (7). e70016 ISSN 1040-0397

DOI: https://doi.org/10.1002/elan.70016

Publisher: Wiley

Version: Published Version

Downloaded from: https://e-space.mmu.ac.uk/641967/

Usage rights: Creative Commons: Attribution 4.0

Additional Information: This is an open access article published in Electroanalysis, by Wiley.

Data Access Statement: The data that support the findings of this study are available from the

corresponding author upon reasonable request.

Enquiries:

If you have questions about this document, contact openresearch@mmu.ac.uk. Please include the URL of the record in e-space. If you believe that your, or a third party's rights have been compromised through this document please see our Take Down policy (available from https://www.mmu.ac.uk/library/using-the-library/policies-and-guidelines)



Check for updates





Exploring the Use of Different Carbon Materials Within Additive Manufactured Electrodes: The Sensing of Carbendazim

Muhzamil A. Khan¹ | Robert D. Crapnell¹ | Elena Bernalte¹ | Bill Logan Riehl² | Samuel J. Rowley-Neale¹ | Craig E. Banks¹

¹Faculty of Science and Engineering, Manchester Metropolitan University, Dalton Building, Chester Street, M1 5GD, Manchester, Great Britain | ²Owens Corning S&T, 2790 Columbus Ave, Granville 43023, Ohio, USA

Correspondence: Craig E. Banks (c.banks@mmu.ac.uk)

Received: 27 March 2025 | Revised: 23 May 2025 | Accepted: 24 June 2025 Funding: Aquacheck and Horizon Europe, Grant/Award Number: 101137990

Keywords: additive manufacturing | carbendazim | carbon materials | electrochemical analysis | electrochemistry

ABSTRACT

Additive manufacturing is emerging as a technology utilised within the field of electrochemistry, where researchers need to understand the electrochemical capabilities of the electrodes produced. One aspect yet to be fully explored is the effect of using different carbon morphologies and how these differences affect the electrochemical performance. It is understood that edge plane defects are the site of electrochemical activity, therefore, quantifying these defect sites will allow for determination of which morphology is most advantageous. Various filaments containing different morphologies were produced in combination with carbon black (CB) using multiwalled carbon nanotubes (MWCNTs), carbon nanotube clusters, and graphite. All electrodes were subject to physicochemical characterisation using scanning electron microscopy, Raman, and X-ray photoelectron spectroscopy. MWCNTs in combination with CB produced a high performing electrically conductive filament, which showed improved electrochemical performance compared to other bespoke filaments with a heterogenous electron transfer of $k^0_{\rm obs}$ of 3.22 (\pm 0.16) x 10^{-3} cm s⁻¹. The filament containing MWCNTs was also found to show the largest density of edge plane sites of 0.81% and was closest to that of a glassy carbon electrode. All electrodes were successfully tested for the detection of carbendazim producing linear ranges between 5 and 40 μ M. The MWCNT filament also exhibited the best electroanalytical performance, showing a limit of detection of 0.26 μ M and limit of quantification of 0.88 μ M, as well as achieving a recovery of 114% in a river water sample. This work proves that the edge plane defect sites are the site of electrochemical activity within additive manufactured electrodes and should be considered when designing new materials.

1 | Introduction

Additive manufacturing, often referred to as 3D printing, is the approach to which a product is made via the sequential addition of thin layers [1]. AM has emerged as a promising technology with a wide range of uses across a multitude of sectors [2]. With an extensive amount of advantages, such as the ability to produce and modify prototypes rapidly, on demand and on-site production, low cost, and low waste, it is apparent why AM has gained an increasing amount of popularity over recent years

[3, 4]. Additive manufacturing electrochemistry has progressed whereby researchers are making their own bespoke filaments from various carbon morphologies [5–10–11], it is therefore important to understand their electrochemical properties. Edge plane sites, also referred to as defect sites, are known to be the site where electrochemical activity occurs [12]. Edge plane theory suggests that different carbon morphologies contain different densities of edge planes and that those which contain more edge planes will exhibit an enhanced electrochemical performance [13].

This is an open access article under the terms of the Creative Commons Attribution License, which permits use, distribution and reproduction in any medium, provided the original work is properly cited.

@ 2025 The Author(s). Electroanalysis published by Wiley-VCH GmbH.

Carbon nanotubes (CNTs) are nanomaterials which have gained an immense amount of attention due to their structural, electronic, and chemical properties [14, 15]. There are two distinct types of nanotubes: single-walled CNTs (SWCNT) and multiwall CNTs (MWCNT). SWCNT are made up of a single sheet of graphite rolled up into a tube with a diameter of 1-2 nm compared to that of the structure of MWCNTs which are composed of concentric and closed graphite tubules, having diameters varying from 2 to 50 nm [16, 17]. It is understood that the ends of the tubes are compared to the edge planes of highly orientated pyrolytic graphite (HOPG), opposed to the walls which are similar in properties to those of the basal planes of HOPG electrodes [18]. The edge plane has been noted to display different electrochemical properties to that of the basal plane. For example, the electrode kinetics at edge plane is significantly faster. A large edge plane/basal plane ratio and rapid electrode kinetics allows for a higher sensitivity and lower limits of detection to be achieved, when incorporated within sensors [19]. Recent work has shown that these electrochemical properties are dependent on the amount of edge plane sites as the edge plane-like sites are the origin for electron transfer [20]. The constant development of nanotubes has led to the increase of novel application, such as batteries [21] and sensors [22]. Furthermore, nanotubes are ideal for nano templates and easily modifiable allowing for further application, such as catalysts, and for hydrogen storage and sensing [23].

Carbon black (CB) is commonly utilised as it possesses a range of properties making it favourable for researchers to employ towards electrochemical applications [24]. Properties include high surface area, electrical conductivity, and electrochemical stability. The structure of CB is made up of particles usually ranging from 10 to 100 nm, which are arranged within a network of interconnected graphene sheets [25]. The complex structure of carbon leads to defect sites, usually towards the edge of the graphene sheets where the structure is seen as less stable and more reactive. These defect sites are often referred to as edge plane sites [26], which show higher surface energy and allows for them to act as active sites for a range of chemical reactions.

Graphite has a layered structure composed of carbon atoms arranged in hexagonal rings. These layers are made up of 2D sheets called graphene which are then stacked on top of each other [27]. The layers can slide past each other easily, giving graphite its lubricating properties. Additionally, the delocalised electrons within the layers contribute to graphite's high electrical conductivity [28]. Graphite plays a crucial role in additive manufacturing electrochemistry due to its ease of integration with various polymers while maintaining desirable properties of both the polymer and graphite which is why it's often used as an electrode material in various electrochemical processes, such as batteries, fuel cells, and electrolysis [29]. Graphite's high electrical conductivity, chemical stability, and large surface area make it an ideal material for facilitating electron transfer reactions at the electrode surface. This makes it valuable in both research and industrial applications within the field of electrochemistry. Edge planes refer to the surfaces of graphite crystals that expose the edges of graphene layers. These edge planes are significantly more reactive than the basal planes due to the presence of unsaturated carbon atoms, which can form bonds more readily [30].

Although, MWCNT, CB, and graphite show plenty of positives, each have their own distinct properties and cost profiles which

must be considered when deciding which is suitable for a specific application. For example, graphite is commonly used due to its low cost, however, it is limited in its surface area and energy density when compared to others [31]. CB has a moderate cost but provides a higher level of conductivity and surface area to that of graphite [32]. MWCNT possesses the superior electrochemical properties and has the best conductivity but comes at a significantly higher price due to the complex production processes [33]. Furthermore, these carbons have shown to exhibit different edge plane percentages in work using carbon paste electrodes, however, these electrodes are not commonly used within electrochemical applications. One area that has seen rapid increase in popularity, within electrochemistry, is additive manufacturing.

Within electrochemistry, additive manufacturing has commonly been utilised to produce a working electrode. Initially, researchers looked to available commercially conductive filaments and used them towards various applications such as for sensing platforms [34], and drug screening [35]. There are various options for commercial filament, though the most used within literature is ProtoPasta. The composition of the filament is known to be primarily poly (lactic acid) (PLA, >65 wt%), as well as also including an unidentified polymer (<12.7 wt%), and the conductive filler of CB (CB, <21.43 wt%) [36]. However, studies have shown that the performance of commercial filaments is not reliable and is very limited due to its low wt% of conductive filler, hence, the development of bespoke filaments acquires high importance. The production of bespoke filament has led to the expansion of how additive-manufactured electrodes can be a viable option, as these filaments are more comparable to traditional electrodes used, like glassy carbon electrodes [5-36-7, 37]. Researchers are becoming aware of the benefits when different carbon morphologies, such as C, graphite, and CB, which have been incorporated within additive-manufactured electrodes. Recently researchers have moved into using mixed carbon allotropes to utilise their specific characteristics, such as MWCNT filament, for improved electrochemical abilities [38], or graphite for a low-cost filament and improved sustainability [5, 6]. As such, understanding of how these nanomaterials work within additive-manufactured electrodes is crucial for the field to mature [5].

In this work, we look to apply edge plane theory previously applied to carbon paste electrodes and translate the methodology to additive-manufactured electrodes to quantify the density of edge plane sites. We will produce four filaments containing different carbon allotropes: MWCNTs, nanotube clusters, graphite, and CB. These filaments will be 3D printed into working electrodes and electrochemically and physiochemically characterised. Moreover, an experiment utilising $\rm MoO_2$ nanowires to block the edge plane sites will be conducted to show the effect that these defect sites have towards the electrochemical activity of the additive manufactured electrodes.

2 | Experimental

2.1 | Chemicals

All chemicals used were of analytical grade and used as received without any further purification. All solutions were prepared

with deionised water of resistivity not less than 18.2 M Ω cm from a Milli-Q Integral 3 system from Millipore UK. Hexaamine ruthenium (III) chloride (98%), potassium ferricyanide (99%), potassium ferrocyanide (98.5%), potassium chloride (99%), castor oil, graphite powder (>20 µm), sodium molybdate dihydrate (99%), sodium chloride (99.5%), ammonium chloride (99.5%), boric acid (99%), acetic acid (>99%), sulphuric acid (99%), and sodium hydroxide pellets (97%) were purchased from Sigma (Gillingham, UK). MWCNT (10–30 µm length, 10–20 nm outer diameter) were purchased from Cheap Tubes (Vermont, USA), carbon nanotube clusters (electrochemical grade 1 µm clusters) which have been previously characterised [39] were purchased from Phoenix NanoSystems (Kettering, OH), CB was purchased from PI-KEM (Tamworth, UK), and recycled poly(lactic acid) (rPLA) was purchased from Gianeco (Turin, Italy).

Inland water samples were used as real samples in this study. Inland waters is a term that defines any area of water not categorised as 'sea' (e.g., canals, tidal and non-tidal rivers, lakes, and some estuarial waters). The river water utilised was obtained in a plastic container from the River Irwell at Burrs Country Park (Bury, UK). The sample was filtered with a $0.45\,\mu m$ filter from Millipore and then stored at room temperature and used within a day of sampling.

2.2 | Filament Production

Prior to any mixing or filament production, all rPLA was dried in an oven at 60°C for a minimum of 2.5 h, which removed any residual water in the polymer. The polymer composition was prepared using 55 wt% rPLA, 10 wt% castor oil, and 35 wt% CB, which was reduced to 21 wt% when 14 wt% MWCNT/ Graphite/ carbon nanotube clusters were incorporated. The compounds were mixed at 190°C with Banbury rotors for 5 min using a Thermo Haake Polydrive dynameter fitted with a Thermo Haake Rheomix 600 (Thermo-Haake, Germany). The resulting polymer composite was allowed to cool to room temperature before being granulated to create a finer granule size using a Rapid Granulator 1528 (Rapid, Sweden). The granulated samples were collected and processed through the hopper of a EX6 extrusion line (Filabot, VA, USA). The molten polymer was extruded from a 1.75 mm die head, pulled along an Airpath cooling line (Filabot, VA, USA). The filaments were then ready to use for AM.

2.3 | Additive Manufacturing of Electrodes

All computer designs and .3MF files in this manuscript were produced using Fusion 360 (Autodesk, CA, USA). These files were sliced and converted to .GCODE files and were taken to for printing by the open-source software, PrusaSlicer (Prusa Research, Prague, Czech Republic). The additive manufactured electrodes were 3D-printed using fused filament fabrication technology on a Prusa i3 MK3S+ (Prusa Research, Prague, Czech Republic). All additive-manufactured electrodes were printed onto polyimide tape using a 0.6 mm nozzle with a nozzle temperature of 215°C and bed temperature of 60°C, 100% rectilinear infill [40], 0.15 mm layer height, and print speed of 35 mm s⁻¹.

2.4 | Physiochemical Characterisation

Scanning electron microscopy (SEM) micrographs were obtained using a Crossbeam 350 Focussed Ion Beam–SEM (Carl Zeiss Ltd., Cambridge, UK) fitted with a field emission electron gun. Imaging was completed using a secondary electron secondary ion detector. Samples were mounted on the aluminium SEM pin stubs (12 mm diameter, Agar Scientific, Essex, UK) using adhesive carbon tabs (12 mm diameter, Agar Scientific, Essex, UK) and coated with a 3 nm layer of Au/Pd metal using a Leica EM ACE200 coating system before imaging. Sputter coating was necessary as although the electrode is conductive, the polymer, which is an insulator, is in a 55 wt% and without sputter coating charging issues on the polymer occur.

Raman spectroscopy was performed on a Renishaw PLC in Via Raman Microscope controlled by WiRE 2 software at a laser wavelength of 514 nm.

X-ray photoelectron spectroscopy (XPS) data were acquired using an AXIS Supra (Kratos, UK), equipped with a monochromated Al X-ray source (1486.6 eV) operating at 225 W and a hemispherical sector analyser. It was operated in fixed transmission mode with a pass energy of 160 eV for survey scans and 20 eV for region scans with the collimator operating in slot mode for an analysis area of approximately $700 \times 300 \,\mu\text{m}$, the full width at half maximum (FWHM) of the Ag 3d5/2 peak using a pass energy of 20 eV was 0.613 eV. Before analysis, each sample was ultrasonicated for 15 min in propan-2-ol and then dried for 2.5 h at 65°C as shown in our unpublished data to remove excess contamination and minimise the risk of misleading data. The binding energy scale was calibrated by setting the graphitic sp^2 C 1s peak to 284.5 eV. This calibration is acknowledged to be flawed but was nonetheless used in the absence of reasonable alternatives, and because only limited information was to be inferred from absolute peak positions.

2.5 | Electrochemical Experiments

All electrochemical measurements were performed on an Autolab 100N potentiostat controlled by NOVA 2.1.6 (Utrecht, the Netherlands). The electrochemical characterisation of the bespoke filament and comparison to the benchmarks were performed using a lollipop design (\emptyset 5 mm disc with 8 mm connection length and 2×1 mm thickness [41]) electrodes alongside an external commercial AglAgCl (3 M KCl) reference electrode with a nichrome wire counter electrode.

Activation of the additive-manufactured electrodes were performed before the electrochemical experiments. This was achieved electrochemically in NaOH. Then, the additive manufactured electrodes were used as a working electrode alongside a nichrome wire coil as a counter electrode and a AglAgCl (3 M KCl) as a reference electrode and place into a 0.5 M NaOH solution. Chronoamperometry was used to activate the additive-manufactured electrodes by applying a set voltage of $+1.4\,\mathrm{V}$ for 200 s, followed by applying $-1.0\,\mathrm{V}$ for 200 s. The additive-manufactured electrodes were then thoroughly rinsed with deionised water and dried under compressed air before further use.

A solution containing 1 mM sodium molybdate (NaMoO₄), in supporting electrolyte 1 M sodium chloride (NaCl) and 1 M ammonium chloride (NH₄Cl), was prepared, and adjusted to a pH of 8.5 with sodium hydroxide (NaOH). A potential of 1.4 V was held during chronoamperometry for 600 s to achieve successful deposition of MoO_2 nanowires upon the additive manufactured electrodes. Following chronoamperometry, the electrodes were rinsed gently with deionised water (as above) to remove excess salt residues [42].

Spiked real water samples were analysed through the external calibration method, where the river water was spiked with $10\,\mu\text{M}$ of carbendazim and diluted in BR buffer (pH = 4, 1:50). Analysis was performed using DPV with the following parameters: start potential = +0.6 V; stop potential = +1.2 V; step potential = 0.05 V; modulation amplitude = 0.08 V; modulation time = 0.05 s; and interval time = 0.5 s. Parameters previously optimised by L.R.G Silva et al. [43].

3 | Results and Discussion

3.1 | Production and Characterisation of Filament

Thermal mixing techniques were used to produce the filaments as outlined in Section 2.2. A 35 wt% of conductive filler mix of CB and nanomaterial was used with a ratio of 21:14 wt%, this ratio has been previously optimised as seen in literature [44–49]. Multiple batches were produced through thermal mixing, which were then extruded into one filament, and characterisation was completed across a large portion of this filament to provide accurate representation. The flexibility of the bespoke filaments was excellent as they would allow for significant bending without breaking. Figure S1A shows the MWCNT filament which was the least flexible of the filaments and would contain parts which

were more brittle. Images for other filaments can be seen in Figure S1B–D. Castor oil was used as a biobased plasticiser in a 10 wt% amount which further contributed towards the sustainability and flexibility of the filaments [50]. The role of the plasticiser is to reduce brittleness, improve processability, and enhance the surface finish of the print, without castor oil in the filament, the ability to produce high quality additive-manufactured electrodes wouldn't be possible [50]. The resistance of the filaments was measured across 10 cm of filament. MWCNT had the lowest resistance of $188\pm17\,\Omega$, followed by CB $281\pm19\,\Omega$, graphite $363\pm21\,\Omega$, and clusters $535\pm71\,\Omega$. This is a significant improvement from the commercial filament, which has a resistance of around 2–3 k Ω . The various filaments were then 3D printed to be used as working electrodes before being characterised by SEM, Raman, and XPS.

First, additive-manufactured electrodes were analysed by XPS. The C 1s region for the MWCNT electrodes can be seen in Figure 1A. A peak at 284.5 eV can clearly be seen, which is associated with the X-ray photoelectron emission by graphitic carbon [51, 52]. The atomic concentration for the graphitic carbon peak of the MWCNT electrodes was found to be the greatest at 9.11%. Graphite had the next largest graphitic peak of 8.21%, followed by CB which had 5.34%, and then, carbon nanotube clusters with a graphitic peak of 4.04%. C 1s data for carbon nanotube clusters, graphite, and CB can be found in Figure S2A-C. SEM surface images without any activation are shown in Figure 1B-E giving insight into the structures of the various carbon morphologies used within the additive-manufactured electrodes and provide detailed images of their specific arrangements. The SEM images also confirmed the presence of these nanomaterials as can clearly be seen, for example in Figure 1B, there is a significant amount of MWCNT protruding from the polymer matrix. These MWCNT range from 10 to 20 nm in length, allowing for them to easily be arrange within the mix. Figure 1C shows the clusters which

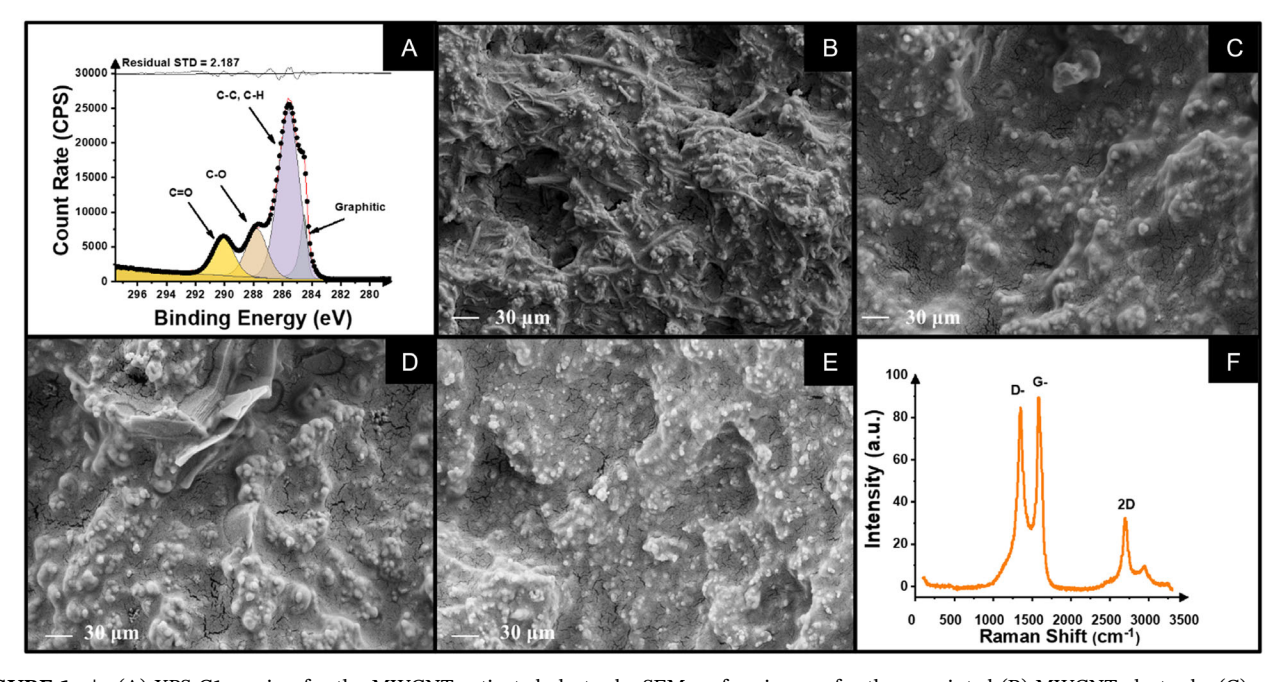


FIGURE 1 (A) XPS C1s region for the MWCNT activated electrode. SEM surface images for the as-printed (B) MWCNT electrode, (C) carbon nanotube clusters electrode, (D) Graphite electrode, and (E) CB electrode. (F) Raman spectroscopy data for MWCNT electrode.

are approximately 20 µm. The mix incorporating graphite is depicted in Figure 1D, where the graphite is >20 µm, as is evident in the image. Raman analysis was next performed on all bespoke filaments in their additive-manufactured electrode forms. Raman spectroscopy data for MWCNT can be found in Figure 1F, which shows the characteristic peaks for graphitic-like structures, with intense peaks at 1338, 1572, and 2680 cm⁻¹ assigned to the D-, G-, and 2D bands, respectively. Figure S3A-C presents Raman spectroscopy data for CB, CNT clusters, and graphite. The D-, and Gbands were seen across all additive-manufactured electrodes, however, the 2D bands were only seen in the MWCNT, carbon nanotube clusters, and CB electrodes, as depicted in Figures 1F, S3A, and S3C. The I_D/I_G ratio for these peaks was calculated to be 0.88 for MWCNT, 0.61 for carbon nanotube clusters, 0.08 for graphite, and 0.87 for CB. Lower ratios indicate fewer defects and a very ordered structure, which indicates the presence of graphite on the surface of the electrode. A higher number indicates towards a less ordered structure and more defects, as seen by MWCNT, carbon nanotube clusters, and CB.

Finally, a contact angle experiment was conducted to determine the hydrophobicity of the electrodes before and after the electrochemical activation procedure. As shown within Figure 2A, when CB electrodes are nonactivated, they are less hydrophilic when compared to Figure 2B where activated CB electrodes are more hydrophilic, causing for the water droplet to no longer sit on the electrode surface. It was observed that the MWCNT electrode was the least hydrophilic with an average contact angle of 99°, whereas graphite was the most hydrophilic with an average contact angle of 87°. The carbon nanotube clusters, and CB electrodes produced contact angles of 91° and 87°, respectively.

3.2 | Electrochemical Characterisation of Additive Manufactured Electrodes

Once physicochemically characterised, the electrochemical properties of the additive-manufactured electrodes were studied. Throughout this study additive manufactured electrodes were only used once, this is due to PLA allowing for significant ingress of water, essentially compromising the electrode after being used [53]. First, the capacitance of an electrode surface can be determined via cyclic voltammetry within a potential window where no faradaic reactions occur. This non-Faradaic region was found to be from 0.2 to 0.4 V for all electrodes. The MWCNT electrode was found to have the highest average

capacitance of $0.32\pm0.06\,\mu\text{F}$, whereas, the CB electrode has the lowest average capacitance of $0.15\pm0.05\,\mu\text{F}$, with the carbon nanotube clusters and graphite producing values of 0.23 ± 0.04 and $0.25\pm0.09\,\mu\text{F}$, respectively.

Second, electrochemical characterisation of the additivemanufactured electrodes was performed against common outer and inner-sphere redox probes 1 mM [Ru (NH₃)₆]³⁺ (in 1 M KCl) and 1 mM [Fe (CN)₆] $^{4-}$ (1M KCl), as shown in Figures 3 and S4. Outer-sphere and inner-sphere probes are crucial for gaining an understanding of redox reaction and the factors influencing electron transfer processes in electrochemical systems. Outer-sphere provides information on how electron transfer occurs through the solvent or electrolyte, whereas inner-sphere allows for understanding of direct interaction between the electrode and redox species. Results of the data were compared to a glassy carbon electrode, edge-plane pyrolytic graphite (EPPG) electrode and commercially available conductive PLA. The heterogenous electron transfer rate constants, $k^0_{\rm obs}$, were calculated as an average of 3 sets of 10 different scan rates experiments recorded from 5 to 500 mV s⁻¹, where each set used a new additive-manufactured electrode. These values were determined using a widely utilised Nicholson method [54] for quasi-reversible electrochemical reactions through (Equation 1) [55]

$$\Psi = k^{0}_{\text{obs}} (\pi D n \nu F / R T)^{-1/2}$$
 (1)

where Ψ is a kinetic parameter, D is the diffusion coefficient ([Ru (NH₃)₆]³⁺ = 9.10 x 10^{-6} cm² s⁻¹ [56], [Fe (CN)₆]^{4-/3-} = 7.26 x 10^{-6} cm² s⁻¹ [57]), n is the number of electrons that

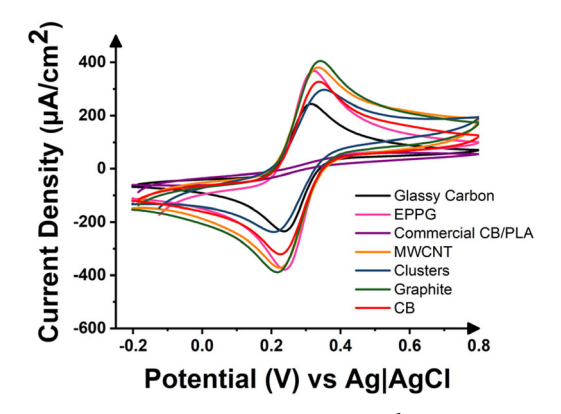


FIGURE 3 | Cyclic voltammogram (50 mV s^{-1}) comparing the glassy carbon, EPPG, commercial CB/PLA, MWCNT, carbon nanotube clusters, graphite, and CB electrodes. Solution: $[\text{Ru (NH}_3)_6]^{3+}$ (1 mM in 1 M KCl).

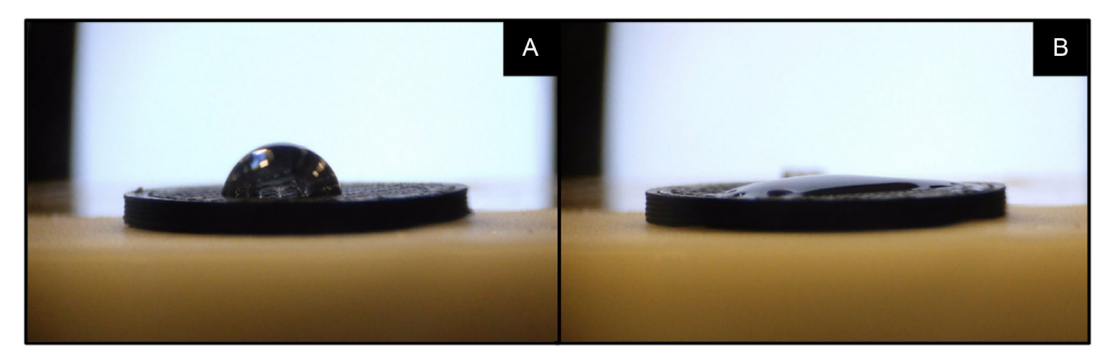


FIGURE 2 | Images of contact angle measurements of CB additive-manufactured electrodes (A) nonactivated and (B) activated.

are taking part in the process (1), F is the faraday constant (96485.3329 C mol⁻¹), ν is the scan rate (5–500 mV s⁻¹), R is the gas constant (8.314 J mol⁻¹ K⁻¹), and T is the temperature in Kelvin (298 K). In order to calculate the heterogeneous electron transfer (HET) rate constant, we use the peak-to-peak separation ($\Delta E_{\rm p}$) to deduce Ψ , where $\Delta E_{\rm p}$ is obtained at various voltammetric scan rates. The heterogenous electron transfer ($k^0_{\rm obs}$) can be calculated via the gradient when plotting Ψ against [$\pi Dnv \ F/RT$] $^{-1/2}$. In cases where $\Delta E_{\rm p}$ is bigger than 212 mV, the following (Equation 2) should be implemented

$$k^{0}_{\text{obs}} = \left[2.18(\alpha DnvF/RT)^{-1/2} \exp\left(-\alpha nvF/RT\right)\Delta E_{p}\right]$$
 (2)

where α is assumed to be 0.5 [58]. The data obtained from these experiments is summarised within Table 1, where it can be seen that the MWCNT has the highest $k^0_{\rm obs}$ of 3.22 (±0.16) x 10^{-3} cm s⁻¹, which is significantly greater than that of the commercially available conductive PLA which had a $k^0_{\rm obs}$ of 4.50 (±1.58) x 10^{-4} cm s⁻¹. It is also clear that the MWCNT additive manufactured electrodes are nearly as good as a glassy carbon electrode, 4.37 (±0.02) x 10^{-3} cm s⁻¹, and EPPG electrode, 4.35 (±0.02) x 10^{-3} cm s⁻¹.

3.3 | Calculation of % Edge Plane Sites

To establish why the MWCNT electrode performs the best, we look to characterise this in terms of edge planes using a method outlined in work published by Hallam et al. [13], which provides a simple

methodology showing the relationship between heterogeneous rate constant and density of defect sites. We can calculate the % of edge plane sites for the additive-manufactured electrodes when used across different redox probes while comparing them to readily available electrodes, through use of (Equation 3). Methodology for (Equation 3) can be found in supplementary information.

$$k^{0}_{\text{obs}} = k^{0}_{\text{edge}} \left(\theta_{\text{edge}} \right) \tag{3}$$

where $k^0_{\rm edge}$ is the electron transfer rate for edge-plane, $\theta_{\rm edge}$ is the coverage of edge plane defects, and $k^0_{\rm obs}$ is the observed electron transfer rate. $k^0_{\rm edge}$ has been rigorously determined with a commercial simulation package providing a value of 0.4 cm s⁻¹ [59].

As seen within Tables 1 and 2, it is apparent that the electrodes containing the MWCNT have the highest amount of edge plane defect sites compared to the other additive-manufactured electrodes (0.81% in [Ru (NH₃)₆]³⁺). These values can be compared to those of the glassy carbon (1.09% in [Ru (NH₃)₆]³⁺) and EPPG electrodes (1.09% in [Ru (NH₃)₆]³⁺). Furthermore, it can be noted that the MWCNT electrodes have significantly more defect sites than that of the commercially available PLA (0.11% in [Ru (NH₃)₆]³⁺). MWCNT exhibits the best electrochemical performance of the additive-manufactured electrodes, this can be explained through the edge plane calculations done which further justifies the importance of the edge plane defect sites. We now look to confirming the edge planes by blocking the sites with use of MoO₂ nanowires and benchmark k^0 _{obs} against bare electrodes.

TABLE 1 | Compilation of data derived from scan rates studies in $[Ru (NH_3)_6]^{3+}$ highlighting the heterogenous electron transfer rate k^0_{obs} , % edge plane density, and electrochemical surface area. (n = 3).

Electrode	$k_{\rm obs}^0$ /cm s ⁻¹ (10 ⁻³)	% Edge (Θ_{edge})	% Electrochemical surface area
Glassy carbon	4.37 (±0.02)	1.09	74 (±1)
EPPG	4.35 (±0.02)	1.09	66 (±2)
Commercial CB/PLA	0.45 (±0.16)	0.11	51 (±9)
MWCNT	3.22 (±0.16)	0.81	100 (±10)
Carbon nanotube clusters	1.45 (±0.04)	0.36	77 (±8)
Graphite	2.90 (±0.01)	0.72	105 (±1)
СВ	2.40 (±0.06)	0.60	75 (±3)

Abbreviations: CB = carbon black; EPPG = edge-plane pyrolytic graphite; MWCNT = multiwalled carbon nanotubes; PLA = poly (lactic acid).

TABLE 2 | Compilation of data derived from scan rates studies in [Fe (CN)₆]4-/3-, highlighting the heterogenous electron transfer rate k^0_{obs} , % edge plane density, and electrochemical surface area (n = 3).

Electrode	$k_{\rm obs}^0$ /cm s ⁻¹ (10 ⁻³)	% Edge (Θ_{edge})	% Electrochemical surface area
Glassy carbon	3.32 (±0.15)	0.83	156 (±21)
EPPG	3.01 (±0.05)	0.75	117 (±22)
Commercial CB/PLA	0.20 (±0.57)	0.05	27 (±7)
MWCNT	2.12 (±0.14)	0.53	211 (±19)
Carbon nanotube clusters	1.59 (±0.15)	0.34	172 (±14)
Graphite	1.92 (±0.13)	0.48	222 (±23)
СВ	1.56 (±0.67)	0.39	186 (±49)

Abbreviations: CB = carbon black; EPPG = edge-plane pyrolytic graphite; MWCNT = multiwalled carbon nanotubes; PLA = poly (lactic acid).

Further testing of the electrochemical performance of the additive-manufactured electrodes was done through cyclic voltammetry against a common inner-sphere probe in [Fe (CN)₆]⁴⁻ as shown within Figure S4. In this instance, all electrodes were activated according to the procedure mentioned in Section 2.5. Unlike outer sphere probes, inner-sphere probes require direct contact with the electrode and the reactant directly coordinates to the electrode surface. Through activation, the surface layer of the polymer is stripped away which in turn creates pores allowing for a direct pathway to the carbon allotropes allowing for an interaction to occur, facilitating electron transfer. Furthermore, the emergence of these pores increases the surface area of the electrode leading to further enhancement in electrochemical response. Again, the MWCNT electrodes outperformed the other additive-manufactured electrodes, as shown by the data presented within Table 2, with a k_{obs}^0 of 2.12 (±0.14) × 10^{-3} cm s⁻¹. This is once again much greater than the $k^0_{
m obs}$ seen with the commercially available conductive PLA, which had a k_{obs}^0 of 2.02 (±0.57)× 10^{-4} cm s⁻¹. MWCNT showed performance at similar levels to the glassy carbon electrode and the EPPG electrode, which had a k^0_{obs} of 3.32 $(\pm 0.14) \times 10^{-3}$ cm s⁻¹ and 3.01 $(\pm 0.05) \times 10^{-3}$ cm s⁻¹, respectively. This data indicates that the MWCNT additivemanufactured electrode can achieve performance levels comparable to traditional electrodes, but at a significantly lower cost.

3.4 | Edge Plane Blocking via Surface Modification with MoO₂ Nanowires

The additive-manufactured electrodes were fabricated with MoO_2 using the method outlined in Section 2.5 [42]. This was

done as it is understood that the MoO2 nanowires would inhibit the edge plane sites. Due to the blockage of these edge plane sites, a subdued electrochemical response is displayed. Visual representation of these surface modifications is shown in Figure S5A-D, which shows SEM images of each electrode type, post modification. In these images, it is clear that fabrication was successful on all electrodes and the surface had been modified. As shown in Figure 4A,C, there is a significant change in peak current when the MoO₂ modified electrodes were tested in $[Ru (NH_3)_6]^{3+}$ compared to the bare electrodes. Analysis of the peak current shows that for the MWCNT electrode the peak current is around six times smaller for the modified electrode, dropping from a peak current of 90.79 µA prior, to 15.32 µA after. Similar can be seen for the graphite electrode where the peak current drops by are 3 times, going from 106.10 to 32.28 µA following modification. In both these instances, peak current is significantly affected following the modification of the surface with the MoO₂ nanowires, showcasing the importance of the edge planes. However, looking at Figure 4B,D, it is noted that there was no significant change between modified and bare electrodes due to the lack of edge plane sites within the carbon nanotube clusters and CB electrodes as previously demonstrated. For the electrodes containing the cluster we can see that the peak heigh goes from 50.52 µA before fabrication to 52.51 µA after fabrication, and for the CB electrode the peak current is 62.61 µA before and 59.36 uA following fabrication, these differences can be deemed as insignificant as they are minimal. The $k^0_{
m obs}$ values reported in Table 3 further confirms the effect of the MoO₂ nanowires, as a smaller value can be seen for the nanotubes and graphite electrodes compared to nonfabricated values, whereas there was little to no changed in k^0_{obs} for the carbon nanotube clusters and CB electrodes.

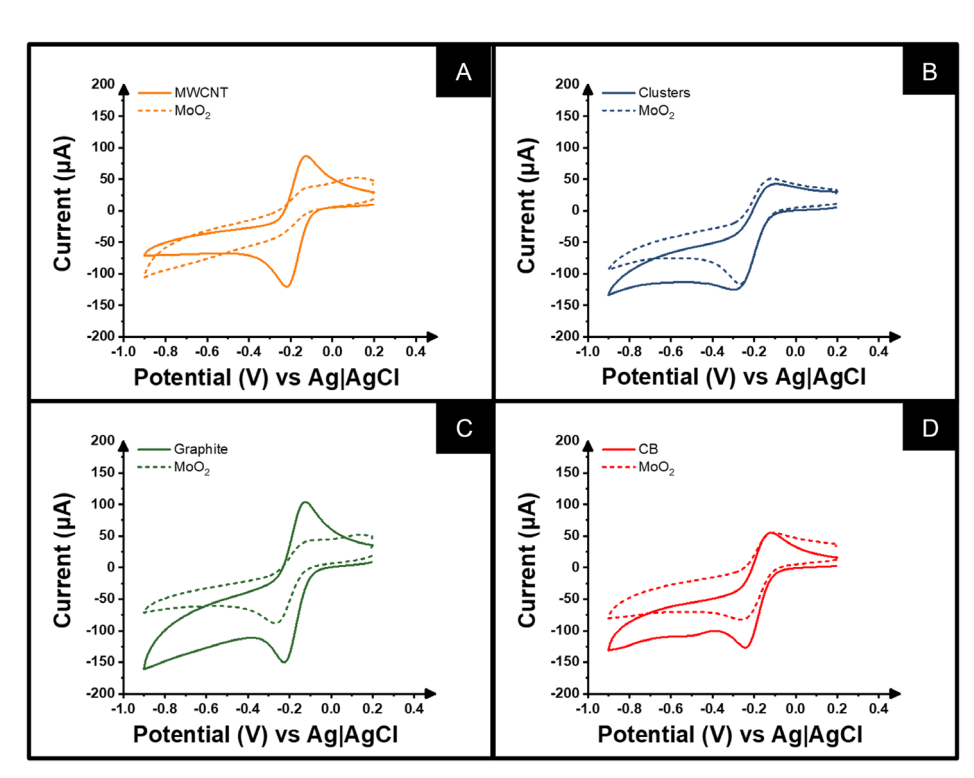


FIGURE 4 | Cyclic voltammogram (50 mV s^{-1}) in $[\text{Ru} (\text{NH}_3)_6]^{3+} (1 \text{ mM in } 1 \text{ M KCl})$ comparing modified and bare electrodes. (A) MWCNT, (B) CNT clusters, (C) graphite, and (D) CB.

TABLE 3 Highlights data for heterogenous electron transfer rate in [Ru (NH3)6]3+ for bare and modified electrodes (n = 3).

Electrode	$k_{\rm obs}^0/{\rm cm~s^{-1}}$ (10 ⁻³)	$k^{0}_{\rm obs}/{\rm cm~s^{-1}}$ (MoO ₂) (10 ⁻³)
MWCNT	3.22 (±0.16)	2.52 (±0.29)
CNT clusters	1.45 (±0.04)	1.88 (±0.55)
Graphite	2.90 (±0.12)	1.93 (±0.19)
СВ	2.40 (±0.06)	2.20 (±0.17)

Abbreviations: CB = carbon black; MWCNT = multiwalled carbon nanotubes

3.5 | Detection of Carbendazim

After electrochemically characterising the electrodes, electrochemical analysis was carried out. This was done by using the additive-manufactured electrodes for the detection of carbendazim, which would provide a quantitative answer for the sensing capabilities of the electrodes. Carbendazim is a fungicide which is used to prevent the growth and spread of fungi as it inhibits fungal cell division, it is often used on crops as it can stop the spread of fungal diseases. However, there are concerns associated with carbendazim, such as reproductive toxicity, potential to contaminate water sources, and its effect on aquatic life. For this reason, the European Union decided to prohibit the use of carbendazim since 2012 [43].

Initially, activated and nonactivated electrodes were tested, and their electroanalytical performance evaluated. In all cases, as shown in Figure 5A–D, the activated electrodes showed greater electrochemical performance compared to the nonactivated electrodes. The activation of the electrode allows for an increase in

surface area, and an increase in adsorption of the active species. The improvement in electrochemical performance can be further supported by looking at improvements of the peak current. For example, in Figure 5B, the peak current improves from 42.97 μA in the nonactivated electrode to 80.44 μA in the activated electrode. The increase in peak current is due to the heightened amount of analyte which is now able to interact with the electrode due to the activation process increasing the surface area.

The electrochemical behaviour of carbendazim was investigated using DPV in 0.04 M BR buffer solution across a pH range from 2.0 to 8.0, as shown in Figure 6A using CB electrodes, and can be seen that peak potentials shifted to more negative values as the pH increased. The relationship of $E_{\rm p}$ versus pH and $I_{\rm p}$ versus pH is shown in Figure 6B, the value from the slope of 0.063 V/pH is close to the theoretical value of 0.059 V/pH, indicating to an equal number of protons and electrons being involved in the oxidation process. It is suggested that the electrochemical oxidation of carbendazim is due to the proposed mechanism of a two-proton and two-electron transfer process, this results in methyl carbamate and an unstable benzimidazole radical being formed, both of which react to form a dimer [60].

Differential pulse voltammetry (DPV) was utilised for the detection of carbendazim at a concentration range between 5 and 40 μ M, shown in Figure 7A for MWCNT. Figure S6A–C shows DPV for carbon nanotube clusters, graphite, and CB. This was the chosen method as DPV provides an enhanced sensitivity and sharper, more well-defined peaks than CV as the differential nature reduces background current and noise, making it a more favourable option for electrochemical analysis. As shown in Table 4, MWCNT was confirmed to be the best electrode as it achieved the lowest limit of detection (LOD) of 0.22 μ M, which

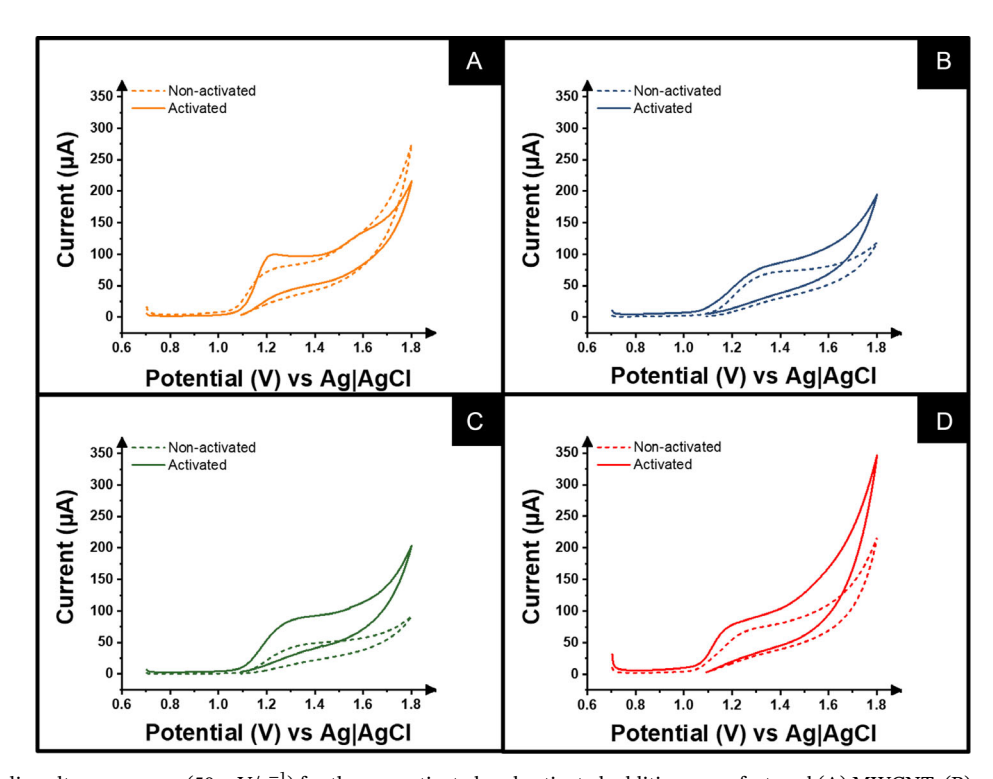


FIGURE 5 | Cyclic voltammograms (50 mV/s^{-1}) for the nonactivated and activated additive manufactured (A) MWCNT, (B) carbon nanotube clusters, (C) graphite, and (D) CB electrodes for the determination of carbendazim (1 mM in 0.04 M Britton-Robinson (BR) buffer pH 4).

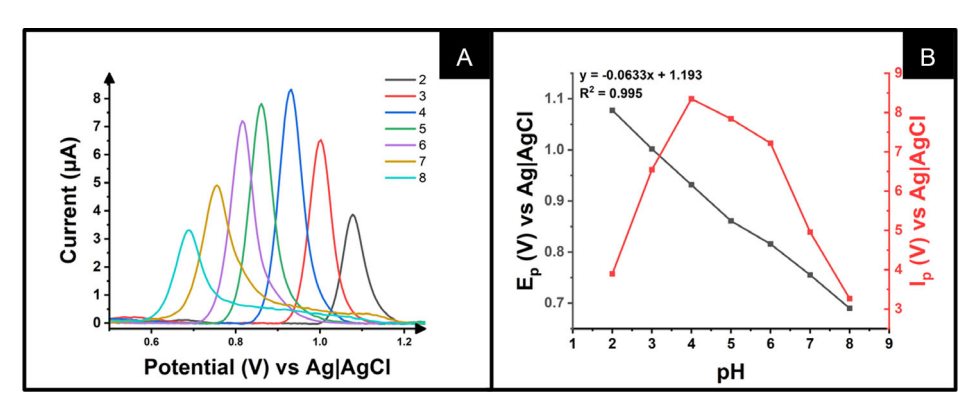


FIGURE 6 | (A) Differential pulse voltammogram of 20 μ M carbendazim in 0.04 M BR buffer solution at different pH values (from 2.0 to 8.0) with a CB electrode. (B) Plot of E_p and I_p vs pH for the carbendazim oxidation process on CB electrode.

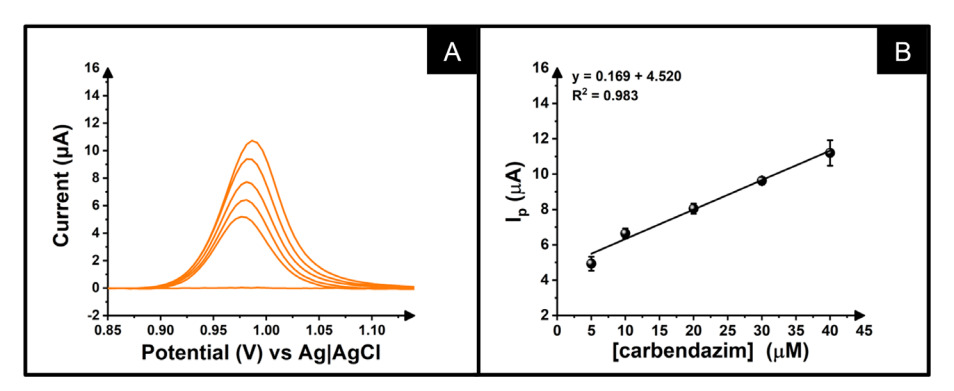


FIGURE 7 | (A) Differential pulse voltammogram for activated MWCNT electrode for the detection of carbendazim in a concentration range of $5-40 \,\mu\text{M}$. (B) Calibration curve for carbendazim using an activated MWCNT electrode.

TABLE 4 | Key data collected from using MWCNT, clusters, graphite, and CB electrodes with differential pulse voltammetry for the detection of carbendazim such as limit of detection, limit of quantification, and sensitivity (n = 3).

Electrode	LOD (µM)	LOQ (μM)	Sensitivity (μΑ μΜ ⁻¹)
MWCNT	0.26	0.88	0.45
Carbon nanotube clusters	4.63	15.40	0.96
Graphite	4.10	13.70	1.39
СВ	7.11	23.69	1.34

Abbreviations: CB = carbon black; MWCNT = multiwalled carbon nanotubes.

is significantly better than the worst electrode, CB, with a LOD of 7.11 μM . LOD was calculated as three times the standard deviation of the blank divided by the slope of the calibration curve. Calibration curve is shown in Figure 7B for MWCNT. Figure S6D–F shows calibration curve for carbon nanotube clusters, graphite, and CB. MWCNT also achieved the lowest limit of quantification (LOQ), 0.88 μM , as well as the highest sensitivity of 0.45 ($\mu A \, \mu M^{-1}$). LOQ was calculated as ten times the standard deviation of the blank divided by the slope of the calibration curve. This further confirms that overall, the MWCNT is the best of the bespoke electrodes which falls in line with the theory as having more edge planes would lead to better electrochemical properties. The results obtained from this study were compared

to the analytical characteristic from works seen throughout literature, this is shown in Table S1.

Finally, the MWCNT electrodes were applied to detect the presence of carbendazim within real spiked river water samples, which resulted in a recovery value of 114%, indicating their applicability for environmental analysis. The successful recovery of carbendazim in river water with additive-manufactured electrodes enables the rapid detection of an illegal, harmful contaminant, as well as ensuring water quality and protecting aquatic life. This work shows the change in response that is seen when different carbon morphologies are used in an electrode. Furthermore, it is highlighted that additive-manufactured electrodes can be used to a high standard comparable to traditional carbon electrodes and are suitable to be used as environmental sensors, providing an alternative approach.

4 | Conclusions

This work reported the fabrication of bespoke conductive filaments using different carbon morphologies in combination with CB to produce additive-manufactured electrodes that were physiochemically and electrochemically characterised for their edge planes defect sites. It was concluded that of the different filaments produced that the MWCNT filament outperformed the other bespoke filaments produced in all aspects. The MWCNT electrodes showed the highest $k^0_{\rm obs}$ and density of edge plane defect

sites in both redox probes tested, $[Ru\ (NH_3)_6]^{3+}$ and $[Fe\ (CN)_6]^{4-}$, compared to carbon nanotube clusters, graphite, and CB.

All bespoke filaments demonstrated enhanced electrochemical performance relative to the commercially available conductive filament obtained from Protopasta, indicating that the tailored material properties and manufacturing processes of the bespoke filaments may be better suited for applications in advanced electrochemical systems, such as sensors. Furthermore, MWCNT exhibited the LOD and LOQ at 0.26 and 0.88 µM, respectively, as well as achieving a carbendazim recovery of 114% in river water samples. This enhanced sensitivity can be attributed to the high density of edge plane defect sites present in MWCNT, which significantly contribute to its enhanced electrochemical performance by facilitating more efficient charge transfer and increasing the active surface area available for electrochemical reactions. Overall, this study successfully demonstrated a method for quantifying the density of edge plane defect sites in 3D-printed electrodes, underscoring the critical role these sites play in influencing the electrochemical behaviour of the materials. By providing a systematic approach to assess these features, the findings enable researchers to further characterise and optimise their electrode materials, ultimately advancing the development of more efficient and effective electrochemical devices for various applications, such as sensors, energy storage, and conversion technologies.

Acknowledgments

The authors would like to thank Hayley Andrews for the acquisition of Raman and SEM data. M.K. would like to thank Aquacheck for the partial funding of his Ph.D. studies. E.B. would like to thank Horizon Europe (grant 101137990).

Conflicts of Interest

The authors declare no conflicts of interest.

Data Availability Statement

The data that support the findings of this study are available from the corresponding author upon reasonable request.

References

- 1. W. K. Swanson and S. Kremer, Three Dimensional Systems, Google Patents (1978).
- 2. M. Pumera, "Three-Dimensionally Printed Electrochemical Systems for Biomedical Analytical Applications," *Current Opinion in Electrochemistry* 14 (2019): 133–137.
- 3. K. R. Ryan, M. P. Down, and C. E. Banks, "Future of Additive Manufacturing: Overview of 4D and 3D Printed Smart and Advanced Materials and Their Applications," *Chemical Engineering Journal* 403 (2021): 126162.
- 4. S. A. Tofail, E. P. Koumoulos, A. Bandyopadhyay, S. Bose, L. O'Donoghue, and C. Charitidis, "Additive Manufacturing: Scientific and Technological Challenges, Market Uptake and Opportunities," *Materials Today* 21 (2018): 22–37.
- 5. I. V. Arantes, R. D. Crapnell, E. Bernalte, M. J. Whittingham, T. R. Paixão, and C. E. Banks, "Mixed Graphite/Carbon Black Recycled PLA Conductive Additive Manufacturing Filament for the Electrochemical Detection of Oxalate," *Analytical Chemistry* 95 (2023): 15086–15093.

- 6. K. K. Augusto, R. D. Crapnell, E. Bernalte, et al., "Optimised Graphite/Carbon Black Loading of Recycled PLA for the Production of Low-Cost Conductive Filament and Its Application to the Detection of β -Estradiol in Environmental Samples," *Microchimica Acta* 191 (2024): 375.
- 7. R. D. Crapnell, I. V. Arantes, J. R. Camargo, et al., "Multi-Walled Carbon Nanotubes/Carbon Black/rPLA for High-Performance Conductive Additive Manufacturing Filament and the Simultaneous Detection of Acetaminophen and Phenylephrine," *Microchimica Acta* 191 (2024): 96.
- 8. J. R. Camargo, R. D. Crapnell, E. Bernalte, et al., "Conductive Recycled PETg Additive Manufacturing Filament for Sterilisable Electroanalytical Healthcare Sensors," *Applied Materials Today* 39 (2024): 102285.
- 9. R. D. Crapnell, E. Bernalte, E. Sigley, and C. E. Banks, "Recycled PETg Embedded with Graphene, Multi-Walled Carbon Nanotubes and Carbon Black for High-Performance Conductive Additive Manufacturing Feedstock," *RSC Advances* 14 (2024): 8108–8115.
- 10. R. D. Crapnell, C. Kalinke, L. R. G. Silva, et al., "Additive Manufacturing Electrochemistry: An Overview of Producing Bespoke Conductive Additive Manufacturing Filaments," *Materials Today* (2023), 71, 73–79.
- 11. D. L. Ramos, R. D. Crapnell, R. Asra, et al., "Conductive Polypropylene Additive Manufacturing Feedstock: Application to Aqueous Electroanalysis and Unlocking Nonaqueous Electrochemistry and Electrosynthesis," *ACS Applied Materials & Interfaces* (2024), 16, 56006–56018.
- 12. C. E. Banks, R. R. Moore, T. J. Davies, and R. G. Compton, "Investigation of Modified Basal Plane Pyrolytic Graphite Electrodes: Definitive Evidence for the Electrocatalytic Properties of the Ends of Carbon Nanotubes," *Chemical Communications* 16 (2004): 1804–1805.
- 13. P. M. Hallam and C. E. Banks, "A Facile Approach for Quantifying the Density of Defects (edge Plane Sites) of Carbon Nanomaterials and Related Structures," *Physical Chemistry Chemical Physics* 13 (2011): 1210–1213.
- 14. C. B. Jacobs, M. J. Peairs, and B. J. Venton, "Carbon Nanotube Based Electrochemical Sensors for Biomolecules," *Analytica Chimica Acta* 662 (2010): 105–127.
- 15. R. D. Crapnell and C. E. Banks, "Electroanalytical Overview: Utilising Micro-and Nano-Dimensional Sized Materials in Electrochemical-Based Biosensing Platforms," *Microchimica Acta* 188 (2021): 1–23.
- 16. R. R. Moore, C. E. Banks, and R. G. Compton, "Basal Plane Pyrolytic Graphite Modified Electrodes: Comparison of Carbon Nanotubes and Graphite Powder as Electrocatalysts," *Analytical Chemistry* 76 (2004): 2677–2682.
- 17. J. Wang, M. Li, Z. Shi, N. Li, and Z. Gu, "Direct Electrochemistry of Cytochrome c at a Glassy Carbon Electrode Modified with Single-Wall Carbon Nanotubes," *Analytical Chemistry* 74 (2002): 1993–1997.
- 18. J. J. Gooding, R. Wibowo, W. Yang Liu, D. Losic, S. Orbons, et al., "Protein Electrochemistry Using Aligned Carbon Nanotube Arrays," *Journal of the American Chemical Society* 125 (2003): 9006–9007.
- 19. S. J. Tans, A. R. Verschueren, and C. Dekker, "Room-Temperature Transistor Based on a Single Carbon Nanotube," *Nature* 393 (1998): 49–52.
- 20. G. Che, B. B. Lakshmi, E. R. Fisher, and C. R. Martin, "Carbon Nanotubule Membranes for Electrochemical Energy Storage and Production," *Nature* 393 (1998): 346–349.
- 21. S.-H. Chung and A. Manthiram, "High-Performance Li-S Batteries with an Ultra-Lightweight MWCNT-Coated Separator," *The Journal of Physical Chemistry Letters* 5 (2014): 1978–1983.

- 22. S. Sharma, S. Hussain, S. Singh, and S. Islam, "MWCNT-Conducting Polymer Composite Based Ammonia Gas Sensors: A New Approach for Complete Recovery Process," *Sensors and Actuators B: Chemical* 194 (2014): 213–219.
- 23. C. E. Banks, R. G. Compton, A. C. Fisher, and I. E. Henley, "The Transport Limited Currents at Insonated Electrodes," *Physical Chemistry Chemical Physics* 6 (2004): 3147–3152.
- 24. F. Arduini, F. D. Giorgio, A. Amine, F. Cataldo, D. Moscone, and G. Palleschi, "Electroanalytical Characterization of Carbon Black Nanomaterial Paste Electrode: Development of Highly Sensitive Tyrosinase Biosensor for Catechol Detection," *Analytical Letters* 43 (2010): 1688–1702.
- 25. F. C. Vicentini, T. A. Silva, and O. Fatibello-Filho, "Carbon Black Electrodes Applied in Electroanalysis," *Current Opinion in Electrochemistry* 43 (2023): 101415.
- 26. F. Arduini, S. Cinti, V. Mazzaracchio, V. Scognamiglio, A. Amine, and D. Moscone, "Carbon Black as an Outstanding and Affordable Nanomaterial for Electrochemical (bio) Sensor Design," *Biosensors and Bioelectronics* 156 (2020): 112033.
- 27. M. Wissler, "Graphite and Carbon Powders for Electrochemical Applications," *Journal of Power Sources* 156 (2006): 142–150.
- 28. D. A. Brownson, D. K. Kampouris, and C. E. Banks, "Graphene Electrochemistry: Fundamental Concepts through to Prominent Applications," *Chemical Society Reviews* 41 (2012): 6944–6976.
- 29. P. Murugan, R. D. Nagarajan, B. H. Shetty, M. Govindasamy, and A. K. Sundramoorthy, "Recent Trends in the Applications of Thermally Expanded Graphite for Energy Storage and Sensors-a Review," *Nanoscale Advances* 3 (2021): 6294–6309.
- 30. A. J. Slate, D. A. Brownson, A. S. A. Dena, G. C. Smith, K. A. Whitehead, and C. E. Banks, "Exploring the Electrochemical Performance of Graphite and Graphene Paste Electrodes Composed of Varying Lateral Flake Sizes," *Physical Chemistry Chemical Physics* 20 (2018): 20010–20022.
- 31. Merck, Graphite <20 μm.
- 32. f. scientific, Carbon Black, Super Plr Conductive..
- 33. CheapTubes, Multi Walled Carbon Nanotubes 10-20 nm.
- 34. R. D. Crapnell, E. Bernalte, A. G.-M. Ferrari, et al., "All-in-One Single-Print Additively Manufactured Electroanalytical Sensing Platforms," *ACS Measurement Science Au* 2 (2021): 167–176.
- 35. P. A. Ferreira, F. M. de Oliveira, E. I. de Melo, et al., "Multi Sensor Compatible 3D-Printed Electrochemical Cell for Voltammetric Drug Screening," *Analytica Chimica Acta* 2021 (1169): 338568.
- 36. Proto-Pasta, Conductive PLA Technical Data Sheet.
- 37. I. V. Arantes, R. D. Crapnell, M. J. Whittingham, E. Sigley, T. R. Paixão, and C. E. Banks, "Additive Manufacturing of a Portable Electrochemical Sensor with a Recycled Conductive Filament for the Detection of Atropine in Spiked Drink Samples," *ACS Applied Engineering Materials* 1 (2023): 2397–2406.
- 38. C. Kalinke, R. D. Crapnell, E. Sigley, et al., "Recycled Additive Manufacturing Feedstocks with Carboxylated Multi-Walled Carbon Nanotubes toward the Detection of Yellow Fever Virus cDNA," *Chemical Engineering Journal* 467 (2023): 143513.
- 39. C. P. Jones, K. Jurkschat, A. Crossley, R. G. Compton, B. L. Riehl, and C. E. Banks, "Use of High-Purity Metal-Catalyst-Free Multiwalled Carbon Nanotubes To Avoid Potential Experimental Misinterpretations," *Langmuir* 23 (2007): 9501–9504.
- 40. E. Bernalte, R. D. Crapnell, O. M. Messai, and C. E. Banks, "The Effect of Slicer Infill Pattern on the Electrochemical Performance of Additively Manufactured Electrodes," *ChemElectroChem* 11 (2024): e202300576.

- 41. R. D. Crapnell, A. Garcia-Miranda Ferrari, M. J. Whittingham, et al., "Adjusting the Connection Length of Additively Manufactured Electrodes Changes the Electrochemical and Electroanalytical Performance," *Sensors* 22 (2022): 9521.
- 42. A. García-Miranda Ferrari, J. L. Pimlott, M. P. Down, S. J. Rowley-Neale, and C. E. Banks, "MoO2 Nanowire Electrochemically Decorated Graphene Additively Manufactured Supercapacitor Platforms," *Advanced Energy Materials* 11 (2021): 2100433.
- 43. R. D. Crapnell, I. V. Arantes, M. J. Whittingham, et al., "Utilising Bio-Based Plasticiser Castor Oil and Recycled PLA for the Production of Conductive Additive Manufacturing Feedstock and Detection of Bisphenol A," *Green Chemistry* 25 (2023): 5591–5600.
- 44. R. Blume, D. Rosenthal, J. P. Tessonnier, H. Li, A. Knop-Gericke, and R. Schlögl, "Characterizing Graphitic Carbon with X-Ray Photoelectron Spectroscopy: A Step-by-Step Approach," *ChemCatChem* 7 (2015): 2871–2881.
- 45. T. R. Gengenbach, G. H. Major, M. R. Linford, and C. D. Easton, "Practical Guides for X-Ray Photoelectron Spectroscopy (XPS): Interpreting the Carbon 1s Spectrum," *Journal of Vacuum Science & Technology A* 39 (2021): 2871–2881.
- 46. R. S. Nicholson, "Theory and Application of Cyclic Voltammetry for Measurement of Electrode Reaction Kinetics," *Analytical Chemistry* 37 (1965): 1351–1355.
- 47. S. J. Rowley-Neale, D. A. Brownson, and C. E. Banks, "Defining the Origins of Electron Transfer at Screen-Printed Graphene-Like and Graphite Electrodes: MoO 2 Nanowire Fabrication on Edge Plane Sites Reveals Electrochemical Insights," *Nanoscale* 8 (2016): 15241–15251.
- 48. F. E. Galdino, C. W. Foster, J. A. Bonacin, and C. E. Banks, "Exploring the Electrical Wiring of Screen-Printed Configurations Utilised in Electroanalysis," *Analytical Methods* 7 (2015): 1208–1214.
- 49. T. Davies, M. Hyde, and R. Compton, Nanotrench Arrays Reveal Insight into Graphite Electrochemistry," *Angewandte Chemie* (International ed in English) 44 (2005): 5121–5126.
- 50. L. R. G. Silva, J. S. Stefano, R. D. Crapnell, C. E. Banks, and B. C. Janegitz, "Additive Manufactured Microfluidic Device for Electrochemical Detection of Carbendazim in Honey Samples," *Talanta Open* 7 (2023): 100213.
- 51. R. D. Crapnell, P. S. Adarakatti, and C. E. Banks, "Electroanalytical Overview: The Sensing of Carbendazim," *Analytical Methods* 15 (2023): 4811–4826.
- 52. T. R. Gengenbach, G. H. Major, M. R. Linford, C. D. Easton, Practical guides for x-ray photoelectron spectroscopy (XPS): Interpreting the carbon 1s spectrum, Journal of Vacuum Science & Technology A, 39 (2021).
- 53. R. J. Williams, T. Brine, R. D. Crapnell, A. G.-M. Ferrari, C. E. Banks, The effect of water ingress on additively manufactured electrodes, *Materials Advances*, 3 (2022): 7632–9.
- 54. R. S. Nicholson, Theory and application of cyclic voltammetry for measurement of electrode reaction kinetics, *Analytical chemistry*, 37 (1965): 1351–5.
- 55. S. J. Rowley-Neale, D. A. Brownson, C. E. Banks, Defining the origins of electron transfer at screen-printed graphene-like and graphite electrodes: MoO 2 nanowire fabrication on edge plane sites reveals electrochemical insights, *Nanoscale*, 8 (2016): 15241–51.
- 56. D. A. C. Brownson, S. A. Varey, F. Hussain, S. J. Haigh, C. E. Banks, Electrochemical properties of CVD grown pristine graphene: monolayer-vs. quasi-graphene, *Nanoscale*, 6 (2014): 1607–21.
- 57. S. J. Konopka, B. McDuffie, Diffusion coefficients of ferri- and ferrocyanide ions in aqueous media, using twin-electrode thin-layer electrochemistry, *Analytical Chemistry*, 42 (1970): 1741–6.

- 58. F. E. Galdino, C. W. Foster, J. A. Bonacin, C. E. Banks, Exploring the electrical wiring of screen-printed configurations utilised in electroanalysis, *Analytical Methods*, 7 (2015): 1208–14.
- 59. T. Davies, M. Hyde, R. Compton, Nanotrench arrays reveal insight into graphite electrochemistry, *Angewandte Chemie (International ed in English)*, 44 (2005).
- 60. R. D. Crapnell, P. S. Adarakatti, C. E. Banks, Electroanalytical overview: the sensing of carbendazim, *Analytical Methods*, 15 (2023): 4811–26.

Supporting Information

Additional supporting information can be found online in the Supporting Information section.